Lab on a Chip

PAPER

View Article Online
View Journal | View Issue

Cite this: *Lab Chip*, 2018, **18**, 2300

An automated microfluidic gene-editing platform for deciphering cancer genes†

Hugo Sinha, [ab] Angela B. V. Quach, [bc] Philippe Q. N. Vo [ab] and Steve C. C. Shih *[abc]

Gene-editing techniques such as RNA-guided endonuclease systems are becoming increasingly popular for phenotypic screening. Such screens are normally conducted in arrayed or pooled formats. There has been considerable interest in recent years to find new technological methods for conducting these gene-editing assays. We report here the first digital microfluidic method that can automate arrayed gene-editing in mammalian cells. Specifically, this method was useful in culturing lung cancer cells for up to six days, as well as implementing automated gene transfection and knockout procedures. In addition, a standardized imaging pipeline to analyse fluorescently labelled cells was also designed and implemented during these procedures. A gene editing assay for interrogating the MAPK/ERK pathway was performed to show the utility of our platform and to determine the effects of knocking out the *RAF1* gene in lung cancer cells. In addition to gene knockout, we also treated the cells with an inhibitor, Sorafenib Tosylate, to determine the effects of enzymatic inhibition. The combination of enzymatic inhibition and guide targeting on device resulted in lower drug concentrations for achieving half-inhibitory effects (IC_{50}) compared to cells treated only with the inhibitor, confirming that lung cancer cells are being successfully edited on the device. We propose that this system will be useful for other types of gene-editing assays and applications related to personalized medicine.

Received 7th May 2018,
Accepted 25th June 2018

DOI: 10.1039/c8lc00470f

rsc.li/loc

Introduction

Recent efforts in cancer characterization are shifting towards a more personalized approach rather than hierarchical classifications based on chemosensitivity experiments.[1] Cancer is a heterogeneous disease that highly differs in genetic makeup and relies on different pathways for survival, which gives rise to a wide-range of potential responses to different anti-cancer agents.[2,3] One method that has been rapidly growing in interest is to use CRISPR-based screens to systematically identify the genes that are required for the survival and proliferation of mammalian cells.[2–9] Such a method enables complete and permanent inactivation of genes and can offer insight into the genetic basis of the disease and lead to the identification of new drug targets.[5,10–13] Several groups have reported successful editing of endogenous genes in cells in culture *via* transfection of plasmid DNA[14] or stable delivery into cells through the use of lentiviruses or other retroviruses.[15] These systems contain the Cas9 gene which can be expressed to target a specific location in the genome by a single guide RNA that complements the target DNA and be used for loss-of function screens aimed at identifying potential drug targets for cancer treatment.[5,10–17]

The most common format for these loss-of-function perturbations is *in vitro* 'pooled' screens[5,11,15] relying on the delivery of Cas9 nucleases and a 'pool' of guide RNAs (sgRNAs) into the cells by transfection or transduction. Pooled libraries enable screens that simultaneously assess the effect of knocking out hundreds to thousands of individual genes at multiple loci in a phenotypic readout, such as proliferation or metastasis assays. Although such developments provide new opportunities for drug target identification and validation, interpretation of results in a pooled format rely on differential representation of guide RNAs after *vs.* before (as assessed by next-generation sequencing) and rely on enrichment of multiple guide RNAs as a validation of target relevance.[11,16] Furthermore, the complexity of population dynamics, each cell being in competition with many others, may contribute to biases resulting in higher relative abundance of some perturbations compared to some others. An alternative to 'pooled' screens is to implement 'arrayed' screens where cells are genetically perturbed only with one known gene

[a] *Department of Electrical and Computer Engineering, Concordia University, Montréal, Québec, Canada. E-mail: steve.shih@concordia.ca; Tel: +1 (514) 848 2424 x7579*
[b] *Centre for Applied Synthetic Biology, Concordia University, Montréal, Québec, Canada*
[c] *Department of Biology, Concordia University, Montréal, Québec, Canada*
† Electronic supplementary information (ESI) available. See DOI: 10.1039/c8lc00470f

target.[18,19] This can potentially enable use of a wider range of cellular phenotypes to be investigated.[20–22] Limitations of arrayed experiments are the associated costs (usually an order of magnitude more expensive than pooled libraries[23]) since they require special facilities that use automation for the handling of plates and the inefficient workflow that includes labor-intensive preparatory work to build and produce individual guide libraries and transferring the samples to other platforms for analysis. Thus, an automated and integrated platform that will culture cells for days, enable efficient handling of mammalian cells and reagents, express the gene editing machinery targeting an individual gene or locus in cells, and assay cell phenotypes will be beneficial for these arrayed-type experiments. This will save on overall costs and improve the workflow by minimizing the time frame between perturbation and measurement.

Arrayed libraries are typically generated in multi-well plates, where each well contains a virus or vector, or reagents with a guide targeting a specific gene. The tools used for these types of experiments, such as automated robotics coupled with flow cytometry, can provide an exploration of complex phenotypes arising from single perturbations. Despite their outstanding features in reducing cell death or limiting off-target mutagenesis associated with editing,[24,25] these techniques suffer from three key limitations. First, available liquid handling technologies, data acquisition equipment and data storage/processing systems have traditionally been expensive and have large footprints that are well outside of the budgetary reach of many laboratories. In addition, the programming software packages are not standardized between laboratories which frequently discourages interdisciplinary scientists and researchers to use robots as it usually requires more time and effort to instruct a robot to perform a task. Second, liquid handlers for cell culture and sample preparation have multiple sources of variability (especially at the nL volumes) which can cause unintended perturbations related to the gene-editing process – *e.g.*, different volumes can alter cell growth resulting in unequal number of cells across wells of a plate. This can pose variability issues with downstream analysis in terms of measuring transfection and knockout efficiencies related to cell density. Third, there is a lack of standardization in assay and in instrument set-up for flow cytometry and especially for how flow data are analyzed and reported. Thus, these approaches may present additional challenges to the already complex procedures of gene editing.

A strategy to alleviate the challenges described above is to use flow-based microfluidics and fluorescent microscopy techniques.[26–28] The development and maturation of these microdevices and optical techniques have been a boon to be used for cell-based assays and genomics.[29–35] Microfluidics allows the manipulation of small volumes of liquids in nanoliter (or smaller) scales in interconnected micron-sized dimension channels and enables the automated delivery of chemical stimulant to cells. The resulting cellular responses can be imaged with fluorescent reporters or fluorescent labelling techniques. For gene-editing assays, this includes delivery of Cas9 into the cells and visualizing them *via* a fluorescence reporter or using flow cytometry techniques to determine if the Cas9 has been delivered into the cell.[36,37] These methods offer an exciting new framework into gene-editing, but do not incorporate two key steps in the gene-editing process. First, the serial nature of flow-based microfluidics present challenges in delivering many reagents (*i.e.* lipids, DNA, culture medium, drugs, *etc.*) needed for the gene-editing process. Indeed, valves can be integrated into the PDMS-based microdevice, but this can be very complicated to setup (in terms of alignment and insertion of tubing) and to operate.[38,39] Second, two key steps in gene editing – cell culturing and analysis have been performed off-chip – *i.e.* the cells have been cultured in flasks and analyzed by flow cytometry. Hence, a standardized automated gene-editing platform that can automate all the steps would improve the workflow.

To address the challenges described above, we report here a new droplet-based method for gene editing called microfluidic Automated CRISPR–Cas9 Editing (ACE) which can automate all the steps for gene-editing – culture, delivery, and analysis. In this work, we report the application of ACE to evaluate the well-characterized mitogen-activated protein kinase or extracellular signal-regulated kinase (MAPK/ERK) pathway[40,41] by editing the Raf-1 gene with and without a Raf-1 inhibitor Sorafenib Tosylate. The results recapitulate what is known about the pathway and its effect on cell viability, but the technique presented here shows that we are capable of conducting an automated gene-editing workflow from cell culturing to analysis with an open-source automation system coupled with a standardized pipeline to analyse the transfected/knockout fluorescent cells. These results (to our knowledge) are the first of their kind and serve as examples of what is possible for the future – a new technique for probing other types of cancer and serve as a platform for *ex vivo* applications relating to personalized medicine that require automated cell culture, transfection, CRISPR–Cas9 editing, and drug inhibition.

Materials & methods

Device fabrication and assembly, automation setup and operation is described in the ESI.†

Reagents and materials

Microfluidic device fabrication reagents and supplies included chromium-coated glass slides with S1811 photoresist from Telic (Valencia, CA), indium tin oxide (ITO)-coated glass slides, R_S = 15–25 Ω (cat no. CG-61IN-S207, Delta Technologies, Loveland CO), FluoroPel PFC1601V from Cytonix LLC (Beltsville, MD), MF-321 positive photoresist developer from Rohm and Haas (Marlborough, MA), CR-4 chromium etchant from OM Group (Cleveland, OH), AZ-300T photoresist stripper from AZ Electronic Materials (Somerville, NJ), DuPont AF from DuPont Fluoroproducts (Wilmington, DE).

Transparency masks for device fabrication were printed from CAD/Art Services (Bandon, OR) and polylactic acid (PLA) material for 3D printing were purchased from Shop3D (Mississauga, ON, Canada). General chemicals for tissue culture were purchased from Wisent Bio Products (Saint-Bruno, QC, Canada). Invitrogen Lipofectamine 3000 transfection reagent was purchased from Thermo Fisher Scientific (Waltham, MA). Unless specified otherwise, general-use chemicals and kits were purchased from Sigma-Aldrich (St. Louis, MO). Plasmids for this study were purchased from Addgene or donated (see Table S1†) and primers were purchased from Invitrogen (Waltham, MA), and genes (438 bp) were synthesized by IDT (Coralville, IA). Sorafenib Tosylate was purchased from Selleckchem (Houston, TX).

Plasmid construction and purification

CRISPR guide RNAs (gRNA) were synthesized (Fig. S1†) by IDT Technologies after being designed *via* the Benchling online platform (https://benchling.com/), and were PCR amplified to create g-blocks flanked with Esp3I type IIS restriction sites (see Table S2† for primers). Individual PCR reactions consisted of 10 μL 5× Phusion buffer, 1 μL dimethylsulfoxide (DMSO), 20 ng template DNA, individual dNTPs and primers to a final concentration of 200 μM and 0.5 μM each respectively, 0.5 μL Phusion polymerase and distilled water up to 50 μL. The following PCR thermocycling conditions were used: initial denaturation at 98 °C for 30 s followed by 35 cycles of denaturation at 98 °C for 10 s, annealing at 55 °C for 30 s and extension at 72 °C for 30 s kb^{-1}, and a final extension step at 72 °C for 10 min. PCR products were loaded into a 0.8% agarose gel in TAE buffer and resolved at 130 V for 30 min. The corresponding bands from a gel (Fig. S2†) were extracted using a gel extraction kit from BioBasic (Markham, ON, Canada). The one-step gRNA cloning method was adapted from the Findlay *et al.* protocol.[42] The gRNAs were assembled *via* restriction digestion/ligation into the All_in_one_CRISPR/Cas9_LacZ backbone containing Esp3I cut sites on both the 3′ and 5′ ends of LacZα gene fragment. Individual reactions consisted of 25 ng of the g-block (10 ng μL^{-1}), 75 ng all_in_one_CRISPR/Cas9_LacZ1 μL BsmBI (10 U μL^{-1}), 1 μL T4 ligase (Thermo Fisher, Waltham, MA), 2 μL T4 buffer and nuclease-free water to 20 μL total. The mixture was incubated in a thermal cycler at 37 °C for 5 min, 16 °C for 10 min, 37 °C for 15 min and 80 °C for 5 min. Assembled products were heat-shock transformed into the LacZα deficient DH5α *E. coli* strain. The transformed products were grown on LB/S-Gal agar blend and assembled products were discriminated by a color bias for colonies – blue colonies contained the LacZα fragment required for S-Gal hydrolysis, whereas white colonies possessed the g-block insert (*i.e.* without the LacZα gene). White colonies were picked and grown overnight before being DNA purified and sent out for sequencing by Eurofins Genomics (Toronto, ON, Canada) (see Fig. S3† for a schematic of the procedure). All constructed plasmids were deposited to the online Addgene repository (Cambridge, MA).

Macro-scale cell culture, transfection, and knockout

Human lung squamous cell carcinoma dual-labeled stable NCI-H1299 cell line was purchased from Genecopoeia, Inc (SL001, Rockville, MD). H1299 cells were grown in RPMI 1640 containing 10% fetal bovine serum with no antibiotics in an incubator at 37 °C with 5% CO_2.

For macroscale transfection experiments, cells were seeded (1.0×10^5 cells per mL) a day before transfection (day 0) to reach 70–80% confluency in 24 well-plates. On day 1, 500 ng μL^{-1} of DNA were pre-mixed with 1 μL of P3000 reagent in 25 μL of Opti-MEM and added to 1.5 μL Lipofectamine 3000 that was pre-mixed in 25 μL Opti-MEM. Lipids were then incubated with the DNA at room temperature for 10 min to form lipid–DNA complexes. The complexes were pipetted into each individual well containing the adhered cells. On day 2, after incubation, the lipid complexes with DNA were removed by aspiration and fresh complete media was replenished into the wells. Cells were stained with Hoechst 33342 and incubated for 30 min on day 3. The cells were imaged with a 20× objective on an Olympus IX73 inverted microscope (Olympus Canada, Mississauga, ON, Canada) that has fluorescence imaging capabilities (Hoechst: λ_{ex} = 350 nm and λ_{em} = 461 nm; GFP: λ_{ex} = 488 nm and λ_{em} = 509 nm; mCherry: λ_{ex} = 585 nm and λ_{em} = 608 nm). Fluorescence images were further analyzed using the CellProfiler transfection pipeline.

For knockout experiments, the cell seeding followed the steps described in the transfection experiments. For transfection (day 1), 600 ng μL^{-1} of assembled pCRISPR plasmid (with the inserted sgRNA) were mixed with the same reagent compositions as above (1 : 10 ratio of lipid complexes to media in wells). After cells were maintained (*i.e.* replaced with fresh media) on day 3, cells were sub-cultured at a 1 : 4 ratio in a new 24-well plate on day 4 by washing the cells with 200 μL of PBS and removing the cells with 150 μL of 0.25% trypsin–EDTA. Following further maintenance on day 5, on day 6 the cells were stained with 1 μM Hoechst 33342 and imaged using the same microscope (and filters) for knockout analysis using the CellProfiler knockout pipeline. Data were tested at $P < 0.05$ for statistical signficance using a Student's *t*-test.

Microfluidic cell culture, transfection, and knockout

DMF was used to automate the protocols required for gene editing including cell seeding, culture, lipid transfection, reagent delivery, staining, washing, and drug inhibition (see Fig. S4† for fabrication procedure, Fig. S5† for automation system; ESI Video†). In all droplet manipulation steps (which was in 'air' instead of oil[43]), the device was oriented in standard configuration, with the top plate on top, while in all incubation steps, the devices were inverted, with the top plate on the bottom and in a 3D-printed humidified chamber (Fig. S6a†). Before seeding cells onto DMF devices (day 0), cell cultures were grown in T-75 flasks and were rinsed with PBS, trypsinized and suspended in 10 mL of complete media. After centrifugation at 1000 × *g* for 5 min, the cell pellet was suspended in 2 mL of complete media (and supplemented

with 0.05% w/v Pluronics F-68) such that the initial concentration of cells is ~1.5×10^6 cells per mL.

To seed and culture cells (day 0), 2 μL of cells at 1.75×10^6 cells per mL in culture medium were pipetted onto the edge of the ITO and actively dispensed using potentials ~200 V_{RMS} and with a frequency of 10 kHz from the reservoirs (size: 5.8 × 5 mm; volume: 4 μL) into 690 nL unit droplets (unit electrodes: 1.6 × 1.6 mm). These droplets were sequentially passively dispensed on each vacant lift-off spot (~1.2 mm dia.) forming 160 nL droplets on the hydrophilic sites. The excess liquid from the spot was actuated to a waste reservoir and removed with a KimWipe. The device was inverted and incubated in a 37 °C incubator with 5% CO_2 overnight allowing the cells to adhere onto the hydrophilic spot. A 7-step actuation sequence was programmed for mixing transfection reagents to form lipid complexes and for delivery (*via* passive dispensing) to each hydrophilic site that contains cells on day 1, as follows: (1) 1 μL of Lipofectamine was diluted in 25 μL of Opti-MEM and premixed and 2 μL was added to a reservoir. (2) 500 ng μL^{-1} of the plasmid DNA to be inserted and 1 μL of P3000 reagent diluted in 25 μL of Opti-MEM was also added to another reservoir. (3) Both reagents were actively dispensed (360 nL each), merged and mixed in a square configuration using 2 × 2 electrodes and incubated for 10 min to form lipid complexes. (4) The lipid complexes were diluted in a 1 : 1 ratio by combining with a 690 nL unit droplet of Opti-MEM. (5) After mixing, the complexes were delivered to the cells *via* passive dispensing 6 × 160 nL and incubated for 24 h overnight. (6) The lipid complexes on the cells were removed by passively dispensing 6 × 160 nL of fresh complete media. (7) After 24 h, 6 × 160 nL of 1 μM Hoechst stain in liquid media was passively dispensed to each well and fluorescence images were acquired to measure transfection efficiency. In transfection optimization experiments, lipid : media ratios in step 4 were changed by performing serial dilutions – by splitting the initial droplet containing the 1 : 1 diluted complexed DNA into two daughter droplets (360 nL each) and mixing it with a unit droplet of liquid media (690 nL). mCherry transfection efficiency was monitored on the device by microscopy, mounting the devices on a custom 3D-printed microscope holder (Fig. S6b†). Fluorescence images were further analyzed using the CellProfiler transfection pipeline.

For assessing GFP knockout efficiency, 2 μL of cells (~1.75×10^6 cells per mL) were pipetted onto the reservoir and a unit droplet was actuated to the vacant lift-off spot. After overnight incubation, the adhered cells were transfected with 600 ng μL^{-1} of pCRISPR (with the inserted sgRNA) following the steps for transfection (steps 1–6). Cells were maintained until day 5 by passively dispensing fresh media daily (6 × 160 nL) to each cell culture site. GFP knock-out was monitored on the device by using microscopy and mounting the devices on a custom 3D-printed microscope holder to ensure healthy cells during image acquisition. On day 5, the microwells were rinsed with PBS followed by 0.25% trypsin–EDTA by passively dispensing a unit droplet across each well. Following incubation at 37 °C for 5 min, the top-plate was disassembled from the bottom-plate and 100 μL of complete media was pipetted directly onto each hydrophilic spot and transferred to an individual well of a 96-well plate and incubated for 2 days. On day 6, 1 μM Hoechst stain in liquid media was added to each well and fluorescence images were acquired to measure knock-out efficiency using the custom CellProfiler knock-out efficiency pipeline.

Cell imaging and CellProfiler pipeline

Top plates bearing stained and fluorescent cells were analyzed using an inverted Olympus microscope. Typically, images were acquired using a Hamamatsu digital camera (Model C1140-42 U) camera with the HC ImageLive software. We typically acquired images using a UV (250 ms exposure time), GFP (500 ms), or mCherry filter set (1000 ms).

Images from the microscope were analysed using the open-source CellProfiler 2.2.0 r9969F42 software package (http://www.cellprofiler.org/).[44] A custom pipeline was developed, including image cropping, identifying individual and overlapping cells from Hoechst-stained and mCherry fluorescent images, counting total number of cells, measuring the size and shape of cells, creating binary images of the cells (*i.e.* black and white images), and comparing knocked-out and non-knocked out cells (UV and GFP channels). For transfection analysis, the pipeline is divided into four modules. In module 1, the software was instructed to smooth the Hoechst-stained image with a Gaussian filter ($\sigma = 1$) and uses the Otsu Global thresholding method to detect objects with diameters of 20–100 pixel units (two classes, threshold correction factor = 0.8). Neighboring pixels are grouped into objects and undesired clumped objects (*i.e.* two close overlapping objects) are declumped using intensity segregation. In module 2, the software was instructed to threshold the mCherry image to select cells that have the plasmid (threshold correction factor = 1) and binarize the image to have black (corresponding to mCherry-negative) and white (mCherry-positive) regions. In module 3, the software was instructed to overlap images from module 1 and 2 where the image from module 2 served as a mask for the identified nuclei in module 1. All the nuclei-stained cells (from module 1) overlapping with an mCherry-positive region (module 2) were retained and counted which gave the total of transfected cells. In module 4, we use the eqn (1):

$$\text{Efficiency (\%)} = [\text{overlapping nuclei/total nuclei}] \times 100\% \quad (1)$$

The result corresponds to the proportion of mCherry-positive nuclei (*i.e.* transfected cells) *versus* the total number or nuclei. Each data point was further corrected from the negative control cells (*i.e.* non-transfected cells) using the same pipeline.

For the knockout pipeline, four similar modules were created to analyse knockout efficiencies. In module 1, the software followed the instructions for the transfection pipeline.

In module 2, a GFP image was thresholded using the Otsu method (two classes, 0.65 threshold correction factor). Module 3 consisted of overlapping the image with the image from module 2 serving as a mask for the image from module 1. Nuclei-stained cells that overlap with GFP-positive cells (90% of its total pixels) were not considered as knocked-out cells. Module 4 followed eqn (1) – total number of knocked out cells from module 3 divided by the total number of cells obtained from module 1 to obtain knockout efficiencies.

MAPK/ERK pathway experiments

MAPK/ERK pathway experiments consisted of two key components: CRISPR–Cas9 genomic disruption of Raf1 and drug inhibition using Sorafenib Tosylate. In the macroscale, 0.75×10^5 cells per mL of H1299 cells were seeded on day 0 in 24-well plates. 600 ng of the pCRISPR plasmid targeting eGFP (control) or *RAF1* was applied to the wells containing the cells on day 1. On day 3, drug conditions were added at different concentrations: 0 μM, 7.5 μM, 15 μM, 30 μM, 60 μM, 120 μM which were diluted in complete media. On day 5, 5 μM Calcein-AM violet stain (λ_{ex} = 408 nm and λ_{em} = 450 nm) diluted in 250 μL fresh serum-free media was added to the cells and incubated at 37 °C for 30 min. The viability of cells was assessed by performing a fluorescence well scan using the CLARIOStar well-plate reader. The measured fluorescence was normalized to the control to determine the % viability.

Similarly, in the microscale, we followed the transfection protocol for seeding cells and the 7-step protocol for transfection of the pCRISPR plasmid containing sgRNA targeting eGFP or Raf-1. The standard step 7 was replaced with step 7a and step 7b. In step 7a, Sorafenib Tosylate in complete media was actively dispensed into unit droplets and then diluted in liquid media to form six different concentrations (0 μM, 7.5 μM, 15 μM, 30 μM, 60 μM, 120 μM) of which one droplet (0.7 μL) was used to passively dispense onto each hydrophilic spot and the other droplet was saved for future dilutions. After all cells were interrogated with the drugs, they were incubated for two days. In step 7b, six unit droplets of 5 μM Calcein-AM violet stain were passively dispensed to the cells and incubated for 30 min in which images were taken to count the cells using a single module imaging pipeline. Calcein-stained image was smoothed with a Gaussian filter (σ = 1) and used the Otsu Global thresholding method to detect objects with diameters of 20–100 pixel units (two classes, threshold correction factor = 1.25). Neighboring pixels are grouped into objects and undesired clumped objects (*i.e.* two close overlapping objects) are declumped using intensity segregation. The counted cells were normalized to the control (*i.e.* cell interrogated with no drugs). All curves were fit with a sigmoid function and probed for statistical significance using an *F*-test in the linear region.

Results and discussion

Digital microfluidic platform for gene-editing

Gene editing techniques have been applied to a wide range of applications, specifically those involving gene silencing or developing gene therapy strategies to cure diseases.[45–47] Such applications would benefit from a miniaturized automated technique that is capable of integrating the gene-editing process on one platform. Here, we present an automated CRISPR-based microfluidic platform that is capable of culturing, editing, and analysing cells. We call this platform "ACE" after the function of this platform – Automated CRISPR Editing.

The ACE platform was developed to automate the processes related to gene-editing and to address the limitations in current techniques to evaluate genes related to a cancer pathway. ACE relies mainly on digital microfluidics (DMF) that will automate the gene-editing processes through its versatile liquid handling operations: dispense, merge, mix, and split droplets. This work builds upon several DMF and cell-culture studies that have established proof-of-principle protocols.[48–51] To our knowledge, this is the first DMF-based technique that is capable of cell culturing, gene editing, and image analysis for lung cancer cells, shown in Fig. 1. Specifically, this platform was tailored to rapidly deliver single-guide RNAs (sgRNA) in an all-in-one pCRISPR plasmid format to effectively knockout targeted genes in lung cancer cells. The device was customized with reservoirs to hold necessary reagents for lipid-mediated transfection and designated regions for incubation, along with a cell culture region to accommodate cell seeding, maintenance, and transfection (Fig. 1a). Genomic disruption can be assessed phenotypically on the same device using a microscopy-based imaging analysis workflow to determine plasmid delivery efficiencies through monitoring fluorescent protein expression and cell viability using various fluorescent dyes. The device comprises of two parallel-plates separated by a 140 μm spacer. The bottom-plate consists of metal-patterned electrodes with dielectric and hydrophobic layers and serves to manipulate the droplets containing the constituents for gene-editing. One of the primary reasons for using DMF in this work is the individual addressability of droplets that allows for controlled automated liquid handling on the device. However, a continuous challenge with DMF is the reproducibility of droplet movement on the device, especially for liquids that are high in viscosity (*e.g.*, complete cell media). To alleviate this challenge, there are studies that introduce chemical additives or an immiscible fluid to prolong droplet movement.[52–54] In this study, one of the primary challenges we initially observed is that droplet movement of protein rich solutions (*e.g.*, suspended cells) are difficult to move after two days of culturing and maintenance (see Fig. S7† for designs). This is problematic given that typical gene-editing phenotypic readouts are usually observable beyond two days. Previous work has shown that changing the electrode shape can enhance the driving force of the droplet.[55,56] Here, we have modified the electrode design such that the boundary between electrodes are interlaced and have added chemical additives in the droplet. We observed that droplet movement was improved and we were able to complete all the droplet movements necessary (~300 total movements for five days) for cell culture

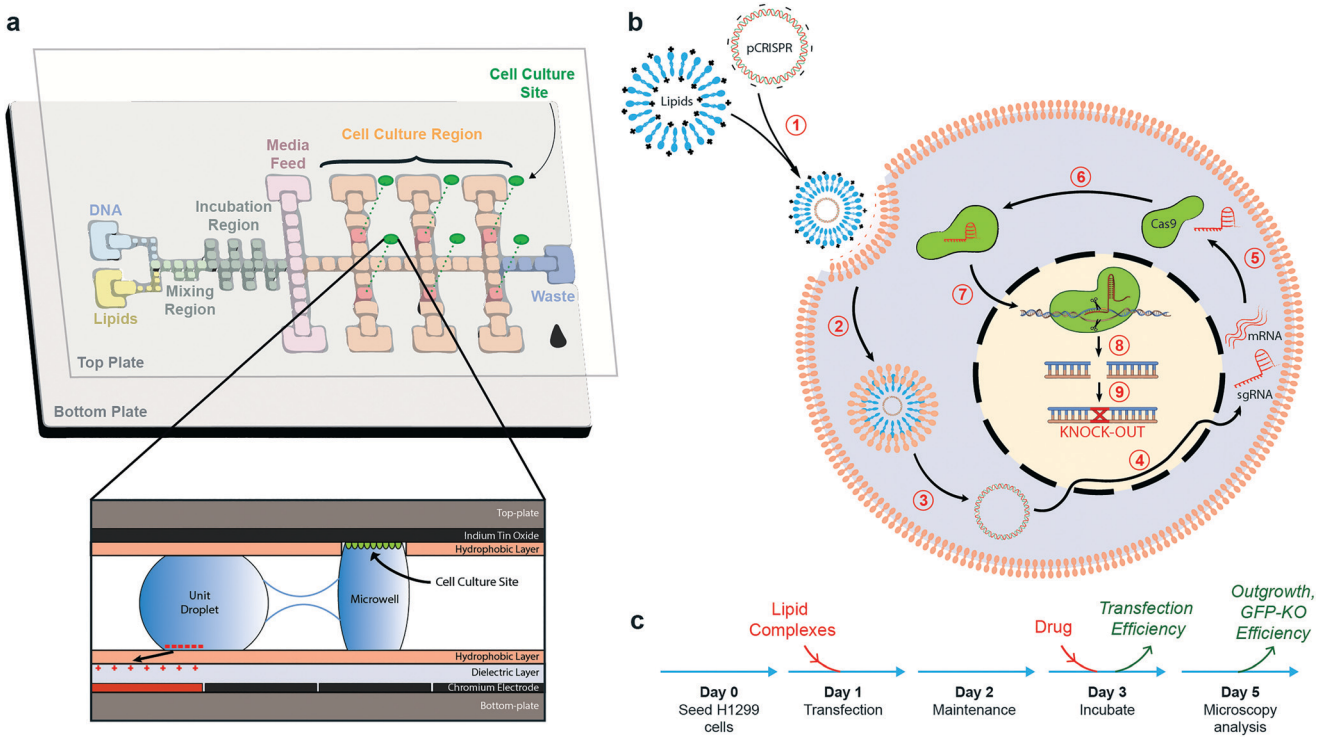

Fig. 1 Digital microfluidics for automated gene-editing assays. (a) Top: A schematic of a digital microfluidic device used for cell culturing, transfection, gene-editing, and analysis. Bottom: Side-view schematic showing adherent cells culture on the top-plate. The cells are transfected using lipid-mediated delivery of plasmids and then measured for knockout by imaging techniques. (b) Step-by-step CRISPR–Cas9 knock-out process at the cellular level. (1) Assembly of DNA–lipid complex, (2) endocytosis, (3) endosomal escape, (4) transduction of Cas9 and sgRNA, (5) translation of Cas9 mRNA, (6) Cas9 ribonucleoprotein assembly, (7) nuclear localization, (8) double-strand break, (9) DNA repair by non-homologous end joining and subsequent genomic disruption by indels. (c) Timeline showing the process of automated gene-editing on chip.

and maintenance, and the gene editing assay. As described in previous studies, the primary reason for this improvement could be due to the overlap of the droplet on the adjacent electrode which increases the applied force on the droplet and thereby increases the velocity of the droplet movement.[57] This will minimize the time a droplet is on an activated electrode which can minimize biofouling on the hydrophobic surface and allow more actuations on the device.

The top-plate is responsible for adherent cell culture and relies on the microfabrication of six 1.2 mm diameter hydrophilic sites. Typically, the cells in suspension are manipulated by applying an electric potential which has shown not to have an effect on cell viability.[58] When moved across the hydrophilic spot, a fraction of the droplet remains pinned to the hydrophilic spot and will serve as the cell culture microvessel – this operation is called "passive dispensing" (Fig. 1a, inset).[48] The delivery of cells to these hydrophilic spots will enable cells to adhere, spread, and proliferate in an upside-down configuration (*i.e.* top plate on the bottom).[59–61] To prevent evaporation, devices are incubated in a 3D printed humidified chamber (Fig. S6a†). After the cells are fixed, the device is flipped to its standard configuration and at designated periods, the cells are transfected with CRIPSR-based plasmids that are complexed in lipid vesicles for efficient delivery of exogenous material to the cells. As shown in Fig. 1b, successful gene-editing in individual cells using our method occurs when cells co-express both the Cas9 and the sgRNA that assemble into a ribonucleoprotein (RNP) complex and is delivered to the nucleus for targeted cleavage. The complex will seek the target sequence, complementary to the seed sequence, using the designed sgRNA and will cleave the target DNA which results in a double stranded break and ideally causes a knockout. For downstream analysis, the cells are incubated and labeled with a fluorescent dye delivered in liquid media by passive dispensing to determine efficiencies of transfection and gene knockout. Using a custom 3D-printed microscope holder (Fig. S6b†), images of the top plate containing cells (without disassembling the device) are captured which can be analysed by CellProfiler to calculate the percentage of transfected or knocked-out cells to the total number of cells.[44] There have been other studies which have cultured adherent cells with DMF, but this is the first time that lung cancer cells have been cultured, edited, and analysed on such a platform. Using the passive dispensing technique, we tested the reproducibility and viability of the lung cancer cells on the hydrophilic spots. A significant amount of trial-and-error was required to ensure cells were healthy and growing to enable gene-editing. Factors such as cell seeding density and microwell culture volume are critical to the maintenance of the cell viability and morphology on the device. Cells were seeded at densities between 1–2 × 10^6 cells per mL and maintained over five days by exchanging

media once per 24 h to sustain viable lung cancer cells with appropriate morphologies. Depending on the assay, the seeding densities were altered to ensure cells were ready for the experiments. For example, for transfection optimization, cells were required to be 70–80% confluent to ensure optimal transfection and therefore we seeded cells at a higher density – 1.75×10^6 cells per mL (see Fig. 1c for gene-editing assay timeline). For longer term experiments – such as knockout experiments which required 5–6 days – cells were seeded at a lower density to achieve the desired confluency for gene editing. At higher densities $>1.5 \times 10^6$ cells per mL, the cells reached confluency quickly, resulting in cell senescence prior to endpoint knock-out efficiency measurements.

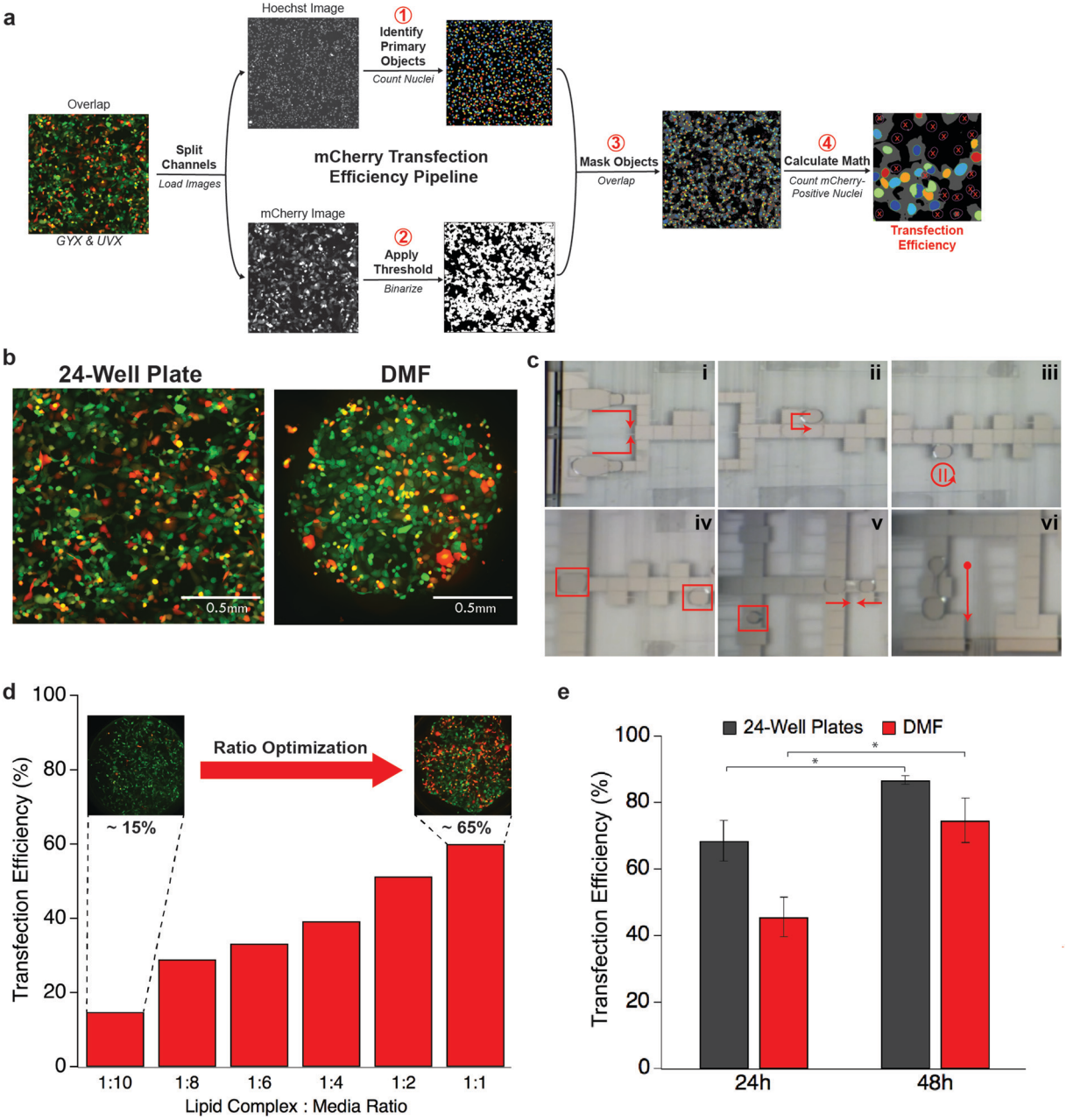

Fig. 2 Lipid-mediated transfection experiments. (a) A schematic showing the imaging pipeline used for analyzing transfection. (b) Microscopy images of mCherry-transfected NCI-H1299 cells in the well-plate format and on DMF devices. (c) A video sequence from ESI Movie† depicting the mixing of lipids and DNA and the passive dispensing procedure onto the hydrophilic spot. Frame (i) shows dispensing of droplets containing DNA and lipids from separate reservoirs and merging both unit droplets. Frame (ii) displays mixing of DNA and lipids on a 2 × 2 electrode array. Frame (iii) shows incubation of complexes for 10 min. Frame (iv) shows the preparation of the dilution by dispensing a droplet of liquid media. Frame (v) show the 1 : 1 dilution of lipid complexes in media. Frame (vi) shows the passive dispensing of dilute lipids onto the cell culture spot. (d) Plot showing the optimization of the lipid complex to media ratio for transfection on device. (e) Plot of the transfection efficiency for a mCherry plasmid in the well-plate and on DMF devices. All plots show error bars with ± 1 s.d, $n = 3$ and $^*P < 0.05$.

Optimizing gene-editing – transfection and knock-out

One of the advantages of digital microfluidics is its compatibility with external equipment and amenability with microscopy techniques for cellular analysis.[52,62–64] In this study, microscopic imaging is used to analyse transfection and gene knockout of lung cancer cells on a DMF platform. Fluorescence-based imaging is enabled by staining with fluorescent dyes or by the integration of fluorescent proteins and the use of reporter genes (*e.g.*, mCherry, GFP) which can also help reveal information about cell state, phenotype and possibly provide some valuable insight on gene expression. As shown in Fig. 2a, two images (using UV and mCherry filters) displaying fluorescently labelled cells are counted, thresholded, and overlapped to measure the transfection efficiency. The simplicity of positioning the top plate on the bottom (such that the top plate was adjacent to the objective) is unique to digital microfluidics since there is no requirement of moving parts or tubing that may interfere with the imaging. Fig. 2b shows a representative image that displays two overlapped fluorescent-labelled images grown on the hydrophilic spot on DMF devices and, for comparison, an overlapped image showing lung cancer cells grown on standard 24 well-plates. As shown, the morphologies of the cultured cells were similar on both surfaces.

For gene-editing assays, transfection is typically a necessary procedure and the successful delivery of sgRNA and Cas9 into cells is critical in producing double-stranded breaks at the target DNA.[65] Lipid-mediated transfection remains popular due to the ease of use, the availability of reagents on the market, and is of reagents on the market and is usually less harmful than electroporation techniques.[66,67] One of the factors that affects cationic lipid-mediated transfection is the bioavailability of lipids assembled with the anionic nucleic acids or the negatively charged proteins, which can be effectively directed to and engulfed by a large proportion of target cells. Concentration of lipid reagents and of nucleic acids are essential to maximize transfection efficiency while minimizing cytotoxicity. Seeking validation of our platform for the transfection of nucleic acids, we generated the lipid–DNA complexes by encapsulating an mCherry plasmid and delivering it to the cells on-chip to optimize transfection and measure the delivery efficiency. A portion of the experiment is depicted in Fig. 2c. Briefly, droplets of diluted lipids and DNA are dispensed, merged, mixed, and incubated. The droplet of complexed DNA–lipids is split and one droplet is used for passive dispensing to transfect the cells while the other droplet is used for further dilutions on the chip. We varied the dilutions of lipid complexes in media from 1 : 1 to 1 : 10 and determined that transfection efficiency is highest (~65%) when a ratio of 1 : 1 is delivered to the cells on chip. Off-chip manufacturer's protocols suggest 1 : 10 ratios as the optimal,[68] however, low efficiencies (~15%) are observed when this ratio is performed on chip (Fig. 2d). We additionally conducted higher ratios (>1 : 10) in well-plates, but observed that this ratio exhibited cytotoxic effects. We hypothesize that the presence of larger quantities of lipids may have cytotoxic effects due to the increase in likelihood in forming higher charge ratio complexes.[69] On device, higher ratios are required to compensate the increase of surface area to volume ratio and enable transfection in microscale conditions. As shown in Fig. 2d (inset images) and Fig. S8,† the morphology of the cells at the 1 : 1 ratio is very similar to the 1 : 10 ratio (and the other ratios) on device and do not show any signs of cell detachment or toxicity. Next, with the optimal ratios for each platform (1 : 10 in well plates, 1 : 1 on device), we assessed the transfection efficiency 24 to 48 h post-transfection. As shown in Fig. 2e, we successfully delivered plasmids encoding mCherry to H1299 cells using our device with transfection efficiencies that were highest after 48 h exhibiting ~74.7% ± 6.8 compared to ~45.7% ± 5.9 after 24 h ($P < 0.05$). We also compared on-chip with well-plate techniques and observed no significant differences ($P > 0.05$) in their efficiencies suggesting that DMF is a suitable alternative platform for transfection.

To test the efficacy of our ACE platform in achieving knockout of endogenous gene targets, we used H1299 cells that stably express enhanced GFP (eGFP) at the AAVS1 harboring sites, where there are no known adverse effects on cells resulting from the inserted DNA fragment.[70] This allows simple phenotypic readouts of gene knock-out using GFP fluorescence to monitor the success of our platform in producing CRISPR-mediated genome editing. Initially, we performed three experiments to test the starting material for transfecting Cas9: (1) directly transfecting the Cas9 protein, (2) co-transfecting plasmids encoding Cas9 only and sgRNAs targeting GFP, and (3) transfecting an all-in-one pCRISPR plasmid containing both the Cas9 and sgRNA. As shown in Fig. S9,† transfecting the all-in-one pCRISPR plasmid enabled high levels of Cas9 expression in 24 h while protein transfection showed lower levels at 24 h. In the Cas9 protein transfected cells, the level of Cas9 protein peaked at the first measured time point 4 h, then rapidly decreased and is barely detectable in the blot after 24 h. Upon realizing favorable expression patterns of the all-in-one pCRISPR plasmid, we opted for this format for three reasons: (1) plasmid DNA is more stable as opposed to RNA and protein, (2) there is generally higher success for transfecting cells with one plasmid that can co-express both the sgRNA and the Cas9 protein as opposed to co-transfection, and (3) the ease by which such plasmids are redesigned (Fig. S2 and S3†). For proof-of-concept knock-out experiments, we targeted the eGFP and cultured and transfected the cells on-chip. We analyzed the knockout using a pipeline similar to the transfection pipeline (Fig. 3a); however, performed the knockout cell analysis off-chip since visualizing the GFP knockout is ~7 days process and during this time the cells are continually proliferating. The high confluency of the cells on day 7 makes counting cells difficult on-chip. After washing and sub-culturing off-chip, a Hoechst stained image and a GFP image (Fig. 3b) are

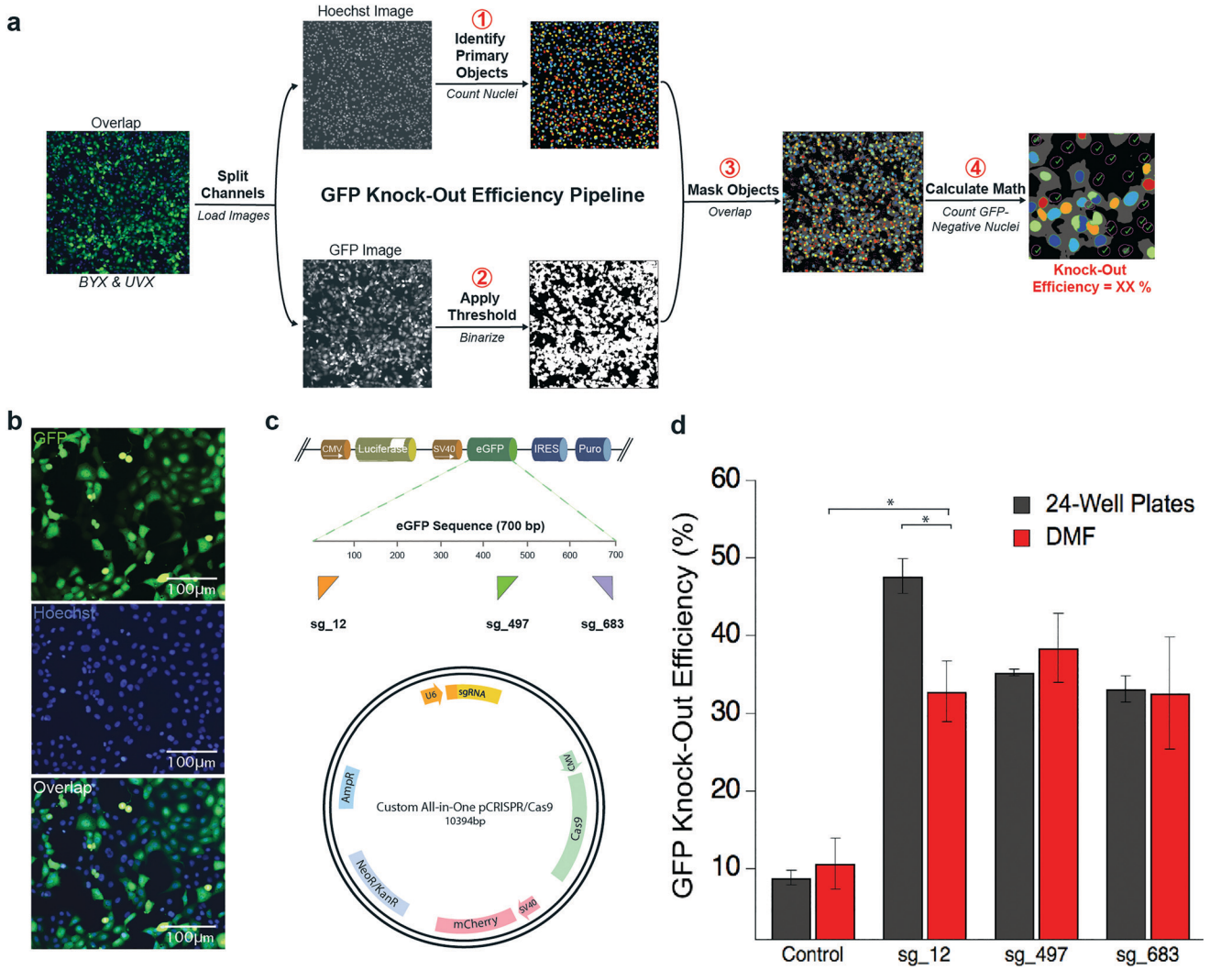

Fig. 3 Knockout of stably integrated eGFP. (a) A schematic showing the imaging pipeline used for analyzing knockout. (b) An image set (Hoechst, GFP, overlap) processed by CellProfiler to assess eGFP knock-out efficiency. (c) Plasmid map of the pCRISPR plasmid used showing the transgene integration in NCI-H1299 and sgRNA target regions of eGFP. (d) Plot shown for the knockout of GFP in well-plates compared to the microscale. Error bars are ± 1 s.d. with $n = 3$ and $*P < 0.05$.

processed by identifying nuclei and thresholding GFP regions – overlapping these images will highlight all the nuclei that are not overlapping GFP-positive regions, thereby being counted as cells exhibiting GFP knock-out. Comparing the number of knock-out nuclei to the total number of nuclei allows for a calculation of GFP knock-out efficiency. We designed and assembled three pCRISPR plasmids that contain an sgRNA targeting different loci in the GFP: upstream (sg_12), middle (sg_497), downstream (sg_683) where the number represents the location of the base pairs for targeting (Fig. 3c). Cells were transfected with a larger pCRISPR plasmid (~10.5 kb), with a reported transfection efficiency similar to a ~5 kb mCherry plasmid (~60% *vs.* 70%, as seen in Fig. S10†) and knockout is observed on day 6. As shown in Fig. 3d, we observed an average efficiency of ~35% on-chip which is comparable to the well-plate experiments ~39% ($P > 0.05$). By analyzing the three different loci, we observe that the knockout efficiencies for the middle and downstream loci using both technologies are very similar. However, we did observe a difference between the upstream loci knockout efficiencies (32.8% *vs.* 47.7%). We hypothesize that this variation is due to the use of well-plates for cell culturing in which adding medium (or any reagent) to the wells can result in uneven distribution, attachment, and growth of cells.[71] This can cause a high variation in counting the cells using the pipeline especially after knockout. However, we observe that there are no differences in the loci (32.8% for sg_12, 38.5% for sg_497, and 32.6% for sg_683) when using DMF and we believe this is attributed to the homogeneity and reproducibility of cell culturing on device.[60] Therefore, this demonstrates the compatibility of DMF for knockout assays related to gene editing.

Evaluating MAPK/ERK pathway

To evaluate the potential of using our platform for gene editing, we explored the relationship between gene function

and cell phenotype by studying a cellular signaling pathway. Cellular signaling is an intricate process driving various cellular activities such as protein synthesis, cell growth and cell senescence, which hold major implications regarding our understanding of tumor cell behavior and progression.[72] Specifically, the MAPK/ERK (or also known as RAS–RAF–MEK–ERK) pathway is a highly conserved signaling cascade that plays a crucial role regulating cell fate decisions and is often upregulated in human cancers.[73,74] The pathway is depicted in Fig. 4a, where a tyrosine receptor kinase serves to relay extracellular signaling to individual cells, through mitogen-activation. *RAS* and *RAF* genes are upstream components of the MAPK/ERK kinase signaling cascade, and therefore are a nodal point in cell proliferation, flagging them as potent oncogenes and natural targets for therapy. Generally, the RAS protein kinase gets phosphorylated and activated and the resulting RAS-GTP will complex with RAF in the plasma membrane. The order of subsequent events is still largely unknown, but a series of phosphorylation and dephosphorylation enable the dimerization of Raf protein kinases, essential for the catalytic activation of RAF.[75,76] Once activated, RAF kinases activate various effector proteins which govern cell proliferation. RAF proteins have been studied for characterization of human cancer – notably RAF1 (also known as c-RAF) was the first isoform to be identified as an oncogene, but interestingly, mutations of *RAF1* are rare in human cancers.[77] Uncertainties surrounding the precise role of RAF1 have driven our interest in studying the effects of disrupting its encoding gene. We initiated this by regulating RAF1 protein expression at both the gene level by CRISPR-mediated knockout and at the protein level by enzyme inhibition using protein inhibitor Sorafenib Tosylate.[78]

To assess the coupled effects of genome editing and drug inhibition, we transfected the H1299 cells with a pCRISPR targeting *RAF1* or a control sgRNA and added 15 μM Sorafenib Tosylate on day 2. Cells with *RAF1* gene editing showed a minimum viability of ~50% on day 4 over a 7-day experiment (Fig. S11†). However, after day 4, cell viability

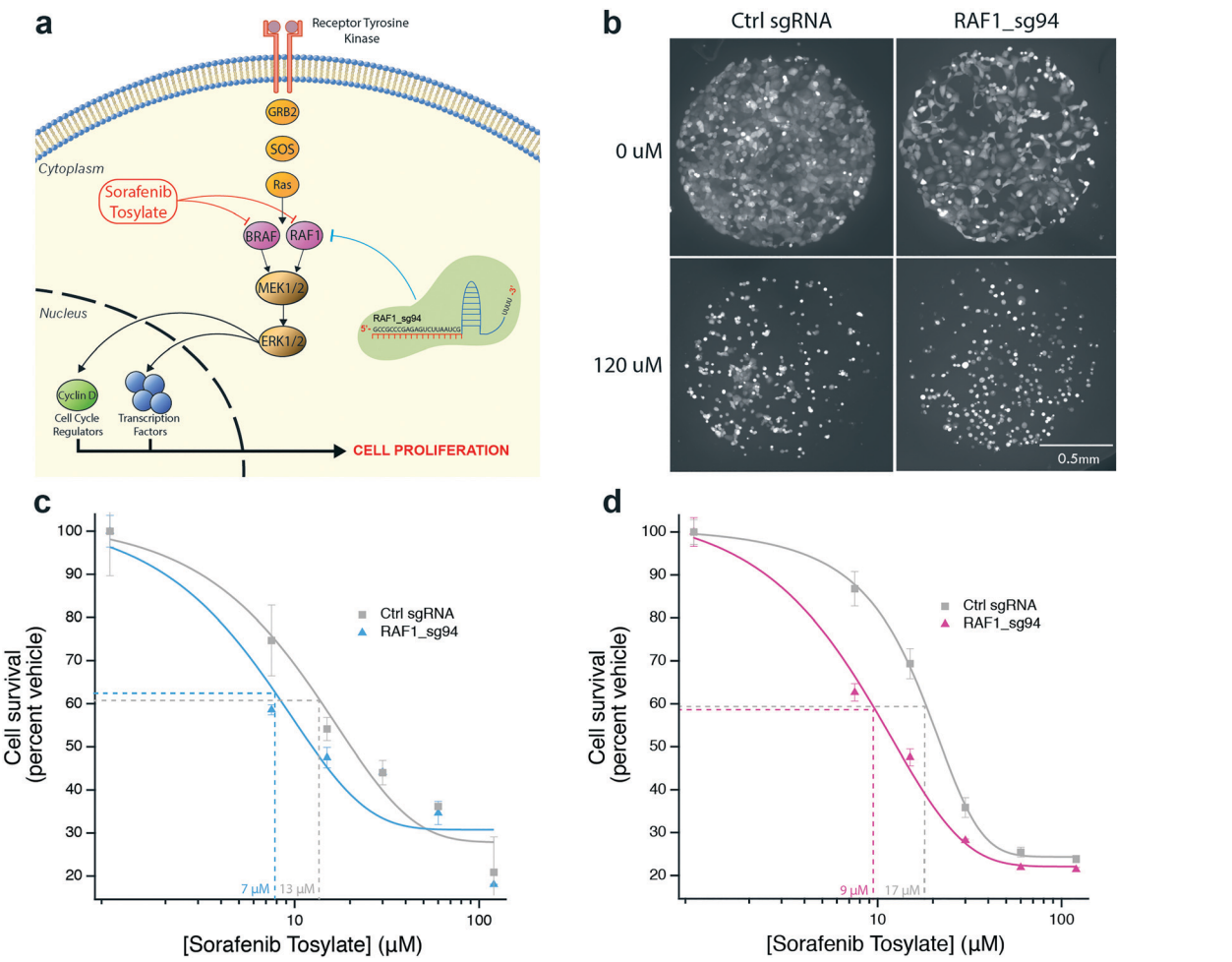

Fig. 4 Identification of cancer genes in the MAPK/ERK pathway. (a) A cartoon illustrating signal transduction in the Ras pathway that leads to eventual cell proliferation. The targeted genes using sgRNAs and the added drug (*i.e.* sorafenib) are indicated on the diagram. (b) Microscopy images of the H1299 cells with sorafenib inhibitor (0 and 120 μM in DMSO) and with guide targeting RAF1 and eGFP (control). (c) On-chip and (d) off-chip dose–response curves for H1299 cells transfected with and without individual guides targeting Raf-1 at different concentrations of sorafenib.

levels started to increase while cells interrogated with both pCRISPR and sorafenib maintained low basal viability levels (~25%) after day 4. We hypothesized that this may be due to the heterogeneity of the cell population after transfection and knock-out or off-target effects caused by the single guide RNA. Evolving the Cas9 enzyme to be more versatile[79] or using other types of RNA-guided endonucleases[80] can perhaps alleviate these lower basal levels and efficiencies.

To verify the effects of targeting *RAF1* by genome editing and enzymatic inhibition, H1299 cells were cultured, edited, assayed and analysed on the ACE platform following procedures for measuring transfection and knockout efficiencies. Here, given the shorter time to obtain a phenotypic readout (5 days), we did not observe the same cell confluency as the GFP knockout experiments and are able to perform the cell analysis on chip. Images of the lung cancer cells that are transfected with and without pCRISPR targeting *RAF1* and treated with the sorafenib inhibitor are analysed using the standardized imaging pipeline (Fig. 4b, Fig. S12†). Fig. 4c shows a dose–response curve for Sorafenib Tosylate (using ACE), illustrating the cell viability of the edited H1299 cells. We examined the effects of RAF protein kinase inhibitor Sorafenib Tosylate with and without CRISPR-mediated *RAF1* targeting. For the case with CRISPR-mediated *RAF1* targeting, the edited H1299 cells showed sensitivity in the linear micromolar range (~7–35 μM) upon treatment of sorafenib (similar to previous studies[81]). In addition, the viability of cells decreased compared to the control. Specifically, the fitted dose–response curve based on the sigmoid equation revealed that the inhibitory sorafenib concentration achieved half-maximal viability level (IC_{50}) at 7.54 μM for the control while there is a ~1.8-fold reduction (13.2 μM) when using pCRISPR targeting *RAF1*. An F-test revealed a significant difference between these two curves for concentrations in the linear regions of the curve (2.5–50 μM) ($P < 0.05$). These on-chip results demonstrate that the addition of the single guide RNA targeting *RAF1* shows a lower dose level to reduce cell viability. These results are also verified using well-plates and we observed similar results through fluorescence well-plate measurements and microscopy images (Fig. 4d; see examples of raw data in Fig. S13†). Moreover, this is the first demonstration of gene-editing on a DMF platform. The ability to edit genes in cancer cells and to detect a phenotypic response highlights the potential of the ACE platform to investigate other pathways using gene-editing techniques.

Conclusion

We present the first demonstration of automated gene editing using digital microfluidics with an application to decipher cancer genes. We characterized the integration of gene-editing with DMF in terms of transfection and knockout efficiencies. A new standardized imaging pipeline was developed for the first time to analyse transfected and knockout cells. A gene-editing assay that targets the *RAF1* gene in the MAPK/ERK pathway was performed to demonstrate the functionality in DMF-cultured lung cancer cells and to highlight a standardized imaging pipeline platform. The combination of automation, DMF, and gene-editing presented here provides a basis for future studies that can potentially analyze a wide range of cancer genes.

Author contributions

H. S. and S. C. C. S designed the experiments. H. S. fabricated the DMF devices and performed cell culturing with the help of A. B. V. Q. and P. Q. N. V. wrote the software to operate the experiments on device. H. S. carried out the experiments and analyzed the data with S. C. C. S. H. S. and S. C. C. S. wrote the paper, and all authors reviewed the final version of the manuscript before submission.

Conflicts of interest

The authors declare no conflict of interest.

Acknowledgements

We thank Vincent Martin's laboratory for donating plasmids and strains and the Centre of Applied Synthetic Biology (CASB) for their technical support. We thank Dr. Alphonsus Ng for his advice on using CellProfiler and Prof. Sylvie Mader for helpful discussions. We thank the Natural Sciences and Engineering Research Council (NSERC), the Fonds de Recherche Nature et technologies (FRQNT), and the Canadian Foundation of Innovation (CFI) for funding. H. S. thanks Concordia University department of Electrical and Computer Engineering for FRS Funding and the Biology Department for academic resources. P. Q. N. V. thanks NSERC and A. B. V. Q thanks NSERC USRA funding.

References

1 A. A. Friedman, A. Letai, D. E. Fisher and K. T. Flaherty, *Nat. Rev. Cancer*, 2015, **15**, 747–756.

2 J. Barretina, G. Caponigro, N. Stransky, K. Venkatesan, A. A. Margolin, S. Kim, C. J. Wilson, J. Lehar, G. V. Kryukov, D. Sonkin, A. Reddy, M. Liu, L. Murray, M. F. Berger, J. E. Monahan, P. Morais, J. Meltzer, A. Korejwa, J. Jane-Valbuena, F. A. Mapa, J. Thibault, E. Bric-Furlong, P. Raman, A. Shipway, I. H. Engels, J. Cheng, G. K. Yu, J. Yu, P. Aspesi, Jr., M. de Silva, K. Jagtap, M. D. Jones, L. Wang, C. Hatton, E. Palescandolo, S. Gupta, S. Mahan, C. Sougnez, R. C. Onofrio, T. Liefeld, L. MacConaill, W. Winckler, M. Reich, N. Li, J. P. Mesirov, S. B. Gabriel, G. Getz, K. Ardlie, V. Chan, V. E. Myer, B. L. Weber, J. Porter, M. Warmuth, P. Finan, J. L. Harris, M. Meyerson, T. R. Golub, M. P. Morrissey, W. R. Sellers, R. Schlegel and L. A. Garraway, *Nature*, 2012, **483**, 603–607.

3 M. J. Garnett, E. J. Edelman, S. J. Heidorn, C. D. Greenman, A. Dastur, K. W. Lau, P. Greninger, I. R. Thompson, X. Luo, J. Soares, Q. Liu, F. Iorio, D. Surdez, L. Chen, R. J. Milano, G. R. Bignell, A. T. Tam, H. Davies, J. A. Stevenson, S. Barthorpe, S. R. Lutz, F. Kogera, K. Lawrence, A. McLaren-

Douglas, X. Mitropoulos, T. Mironenko, H. Thi, L. Richardson, W. Zhou, F. Jewitt, T. Zhang, P. O'Brien, J. L. Boisvert, S. Price, W. Hur, W. Yang, X. Deng, A. Butler, H. G. Choi, J. W. Chang, J. Baselga, I. Stamenkovic, J. A. Engelman, S. V. Sharma, O. Delattre, J. Saez-Rodriguez, N. S. Gray, J. Settleman, P. A. Futreal, D. A. Haber, M. R. Stratton, S. Ramaswamy, U. McDermott and C. H. Benes, *Nature*, 2012, **483**, 570–575.

4 T. Wang, K. Birsoy, N. W. Hughes, K. M. Krupczak, Y. Post, J. J. Wei, E. S. Lander and D. M. Sabatini, *Science*, 2015, **350**, 1096–1101.

5 T. Wang, J. J. Wei, D. M. Sabatini and E. S. Lander, *Science*, 2014, **343**, 80–84.

6 O. Shalem, N. E. Sanjana, E. Hartenian, X. Shi, D. A. Scott, T. Mikkelson, D. Heckl, B. L. Ebert, D. E. Root, J. G. Doench and F. Zhang, *Science*, 2014, **343**, 84–87.

7 N. E. Sanjana, O. Shalem and F. Zhang, *Nat. Methods*, 2014, **11**, 783–784.

8 H. Koike-Yusa, Y. Li, E. P. Tan, C. Velasco-Herrera Mdel and K. Yusa, *Nat. Biotechnol.*, 2014, **32**, 267–273.

9 L. A. Gilbert, M. A. Horlbeck, B. Adamson, J. E. Villalta, Y. Chen, E. H. Whitehead, C. Guimaraes, B. Panning, H. L. Ploegh, M. C. Bassik, L. S. Qi, M. Kampmann and J. S. Weissman, *Cell*, 2014, **159**, 647–661.

10 N. E. Sanjana, O. Shalem and F. Zhang, *Nat. Methods*, 2014, **11**, 783–784.

11 O. Shalem, N. E. Sanjana, E. Hartenian, X. Shi, D. A. Scott, T. S. Mikkelsen, D. Heckl, B. L. Ebert, D. E. Root, J. G. Doench and F. Zhang, *Science*, 2014, **343**, 84–87.

12 L. Cong, F. A. Ran, D. Cox, S. Lin, R. Barretto, N. Habib, P. D. Hsu, X. Wu, W. Jiang, L. A. Marraffini and F. Zhang, *Science*, 2013, **339**, 819–823.

13 F. A. Ran, P. D. Hsu, J. Wright, V. Agarwala, D. A. Scott and F. Zhang, *Nat. Protoc.*, 2013, **8**, 2281–2308.

14 P. S. Choi and M. Meyerson, *Nat. Commun.*, 2014, **5**, 3728.

15 S. Konermann, M. D. Brigham, A. E. Trevino, J. Joung, O. O. Abudayyeh, C. Barcena, P. D. Hsu, N. Habib, J. S. Gootenberg, H. Nishimasu, O. Nureki and F. Zhang, *Nature*, 2015, **517**, 583–588.

16 S. Chen, N. E. Sanjana, K. Zheng, O. Shalem, K. Lee, X. Shi, D. A. Scott, J. Song, J. Q. Pan, R. Weissleder, H. Lee, F. Zhang and P. A. Sharp, *Cell*, 2015, **160**, 1246–1260.

17 R. J. Platt, S. Chen, Y. Zhou, M. J. Yim, L. Swiech, H. R. Kempton, J. E. Dahlman, O. Parnas, T. M. Eisenhaure, M. Jovanovic, D. B. Graham, S. Jhunjhunwala, M. Heidenreich, R. J. Xavier, R. Langer, D. G. Anderson, N. Hacohen, A. Regev, G. Feng, P. A. Sharp and F. Zhang, *Cell*, 2014, **159**, 440–455.

18 P. D. Hsu, D. A. Scott, J. A. Weinstein, F. A. Ran, S. Konermann, V. Agarwala, Y. Li, E. J. Fine, X. Wu, O. Shalem, T. J. Cradick, L. A. Marraffini, G. Bao and F. Zhang, *Nat. Biotechnol.*, 2013, **31**, 827–832.

19 J. G. Doench, N. Fusi, M. Sullender, M. Hegde, E. W. Vaimberg, K. F. Donovan, I. Smith, Z. Tothova, C. Wilen, R. Orchard, H. W. Virgin, J. Listgarten and D. E. Root, *Nat. Biotechnol.*, 2016, **34**, 184–191.

20 B. Neumann, M. Held, U. Liebel, H. Erfle, P. Rogers, R. Pepperkok and J. Ellenberg, *Nat. Methods*, 2006, **3**, 385–390.

21 J. Moffat, D. A. Grueneberg, X. Yang, S. Y. Kim, A. M. Kloepfer, G. Hinkle, B. Piqani, T. M. Eisenhaure, B. Luo, J. K. Grenier, A. E. Carpenter, S. Y. Foo, S. A. Stewart, B. R. Stockwell, N. Hacohen, W. C. Hahn, E. S. Lander, D. M. Sabatini and D. E. Root, *Cell*, 2006, **124**, 1283–1298.

22 S. A. Hasson, L. A. Kane, K. Yamano, C. H. Huang, D. A. Sliter, E. Buehler, C. Wang, S. M. Heman-Ackah, T. Hessa, R. Guha, S. E. Martin and R. J. Youle, *Nature*, 2013, **504**, 291–295.

23 O. Shalem, N. E. Sanjana and F. Zhang, *Nat. Rev. Genet.*, 2015, **16**, 299–311.

24 L. A. Lonowski, Y. Narimatsu, A. Riaz, C. E. Delay, Z. Yang, F. Niola, K. Duda, E. A. Ober, H. Clausen, H. H. Wandall, S. H. Hansen, E. P. Bennett and M. Frodin, *Nat. Protoc.*, 2017, **12**, 581–603.

25 P. D. Hsu, D. A. Scott, J. A. Weinstein, F. A. Ran, S. Konermann, V. Agarwala, Y. Q. Li, E. J. Fine, X. B. Wu, O. Shalem, T. J. Cradick, L. A. Marraffini, G. Bao and F. Zhang, *Nat. Biotechnol.*, 2013, **31**, 827–832.

26 M. R. Bennett, W. L. Pang, N. A. Ostroff, B. L. Baumgartner, S. Nayak, L. S. Tsimring and J. Hasty, *Nature*, 2008, **454**, 1119–1122.

27 T. A. Moore and E. W. Young, *Biomicrofluidics*, 2016, **10**, 044105.

28 P. Paie, F. Bragheri, D. Di Carlo and R. Osellame, *Microsyst. Nanoeng.*, 2017, **3**(1), 1–16.

29 S. H. Au, B. D. Storey, J. C. Moore, Q. Tang, Y. L. Chen, S. Javaid, A. F. Sarioglu, R. Sullivan, M. W. Madden, R. O'Keefe, D. A. Haber, S. Maheswaran, D. M. Langenau, S. L. Stott and M. Toner, *Proc. Natl. Acad. Sci. U. S. A.*, 2016, **113**, 4947–4952.

30 S. Upadhyaya and P. R. Selvaganapathy, *Lab Chip*, 2010, **10**, 341–348.

31 J. T. Nevill, R. Cooper, M. Dueck, D. N. Breslauer and L. P. Lee, *Lab Chip*, 2007, **7**, 1689–1695.

32 F. Lan, B. Demaree, N. Ahmed and A. R. Abate, *Nat. Biotechnol.*, 2017, **35**, 640–646.

33 M. Marimuthu, N. Rousset, A. St-Georges-Robillard, M. A. Lateef, M. Ferland, A. M. Mes-Masson and T. Gervais, *Lab Chip*, 2018, **18**, 304–314.

34 G. Linshiz, N. Stawski, G. Goyal, C. Bi, S. Poust, M. Sharma, V. Mutalik, J. D. Keasling and N. J. Hillson, *ACS Synth. Biol.*, 2014, **3**, 515–524.

35 C. Pak, N. S. Callander, E. W. K. Young, B. Titz, K. Kim, S. Saha, K. Chng, F. Asimakopoulos, D. J. Beebe and S. Miyamoto, *Integr. Biol.*, 2015, **7**, 643–654.

36 X. Han, Z. Liu, M. C. Jo, K. Zhang, Y. Li, Z. Zeng, N. Li, Y. Zu and L. Qin, *Sci. Adv.*, 2015, **1**, e1500454.

37 X. Han, Z. Liu, L. Zhao, F. Wang, Y. Yu, J. Yang, R. Chen and L. Qin, *Angew. Chem., Int. Ed.*, 2016, **55**, 8561–8565.

38 R. Gomez-Sjoberg, A. A. Leyrat, D. M. Pirone, C. S. Chen and S. R. Quake, *Anal. Chem.*, 2007, **79**, 8557–8563.

39 W. Gu, X. Y. Zhu, N. Futai, B. S. Cho and S. Takayama, *Proc. Natl. Acad. Sci. U. S. A.*, 2004, **101**, 15861–15866.

40 A. B. Vojtek and C. J. Der, *J. Biol. Chem.*, 1998, **273**, 19925–19928.
41 J. G. Paez, P. A. Janne, J. C. Lee, S. Tracy, H. Greulich, S. Gabriel, P. Herman, F. J. Kaye, N. Lindeman, T. J. Boggon, K. Naoki, H. Sasaki, Y. Fujii, M. J. Eck, W. R. Sellers, B. E. Johnson and M. Meyerson, *Science*, 2004, **304**, 1497–1500.
42 S. D. Findlay, K. M. Vincent, J. R. Berman and L. M. Postovit, *PLoS One*, 2016, **11**, 0153901.
43 S. K. Fan, P. W. Huang, T. T. Wang and Y. H. Peng, *Lab Chip*, 2008, **8**, 1325–1331.
44 A. E. Carpenter, T. R. Jones, M. R. Lamprecht, C. Clarke, I. H. Kang, O. Friman, D. A. Guertin, J. H. Chang, R. A. Lindquist, J. Moffat, P. Golland and D. M. Sabatini, *Genome Biol.*, 2006, **7**, R100.
45 Y. Zhang, X. Zhan, S. Peng, Y. Cai, Y. S. Zhang, Y. Liu, Z. Wang, Y. Yu, Y. Wang, Q. Shi, X. Zeng, K. Yuan, N. Zhou, R. Joshi, M. Zhang, Z. Zhang and W. Min, *Nanomedicine*, 2018, **14**(5), 1679–1693.
46 A. Sharei, J. Zoldan, A. Adamo, W. Y. Sim, N. Cho, E. Jackson, S. Mao, S. Schneider, M. J. Han, A. Lytton-Jean, P. A. Basto, S. Jhunjhunwala, J. Lee, D. A. Heller, J. W. Kang, G. C. Hartoularos, K. S. Kim, D. G. Anderson, R. Langer and K. F. Jensen, *Proc. Natl. Acad. Sci. U. S. A.*, 2013, **110**, 2082–2087.
47 K. A. Whitehead, R. Langer and D. G. Anderson, *Nat. Rev. Drug Discovery*, 2009, **8**, 129–138.
48 I. A. Eydelnant, U. Uddayasankar, B. Li, M. W. Liao and A. R. Wheeler, *Lab Chip*, 2012, **12**, 750–757.
49 A. H. Ng, B. B. Li, M. D. Chamberlain and A. R. Wheeler, *Annu. Rev. Biomed. Eng.*, 2015, **17**, 91–112.
50 A. P. Aijian and R. L. Garrell, *J. Lab. Autom.*, 2015, **20**, 283–295.
51 D. Witters, N. Vergauwe, S. Vermeir, F. Ceyssens, S. Liekens, R. Puers and J. Lammertyn, *Lab Chip*, 2011, **11**, 2790–2794.
52 S. H. Au, P. Kumar and A. R. Wheeler, *Langmuir*, 2011, **27**, 8586–8594.
53 D. F. do Nascimento, L. R. Arriaga, M. Eggersdorfer, R. Ziblat, F. Marques Mde, F. Reynaud, S. A. Koehler and D. A. Weitz, *Langmuir*, 2016, **32**, 5350–5355.
54 V. N. Luk, G. C. H. Mo and A. R. Wheeler, *Langmuir*, 2008, **24**, 6382–6389.
55 J. F. Chen, Y. H. Yu, J. Li, Y. J. Lai and J. Zhou, *Appl. Phys. Lett.*, 2012, **101**, 234102.
56 L. S. Jang, C. Y. Hsu and C. H. Chen, *Biomed. Microdevices*, 2009, **11**, 1029–1036.
57 M. Abdelgawad, P. Park and A. R. Wheeler, *J. App. Phys.*, 2009, **105**, 094506.
58 S. H. Au, R. Fobel, S. P. Desai, J. Voldman and A. R. Wheeler, *Integr. Biol.*, 2013, **5**, 1014–1025.
59 S. C. C. Shih, I. Barbulovic-Nad, X. N. Yang, R. Fobel and A. R. Wheeler, *Biosens. Bioelectron.*, 2013, **42**, 314–320.
60 S. Srigunapalan, I. A. Eydelnant, C. A. Simmons and A. R. Wheeler, *Lab Chip*, 2012, **12**, 369–375.
61 I. A. Eydelnant, B. B. Li and A. R. Wheeler, *Nat. Commun.*, 2014, **5**, 3355.
62 P. T. Kumar, K. Vriens, M. Cornaglia, M. Gijs, T. Kokalj, K. Thevissen, A. Geeraerd, B. P. A. Cammue, R. Puers and J. Lammertyn, *Lab Chip*, 2015, **15**, 1852–1860.
63 B. F. Bender, A. P. Aijian and R. L. Garrell, *Lab Chip*, 2016, **16**, 1505–1513.
64 M. C. Husser, P. Q. N. Vo, H. Sinha, F. Ahmadi and S. C. C. Shih, *ACS Synth. Biol.*, 2018, **7**, 933–944.
65 F. A. Ran, P. D. Hsu, J. Wright, V. Agarwala, D. A. Scott and F. Zhang, *Nat. Protoc.*, 2013, **8**, 2281–2308.
66 T. K. Kim and J. H. Eberwine, *Anal. Bioanal. Chem.*, 2010, **397**, 3173–3178.
67 S. L. Li, *Curr. Gene Ther.*, 2004, **4**, 309–316.
68 X. Yu, X. Liang, H. Xie, S. Kumar, N. Ravinder, J. Potter, X. de Mollerat du Jeu and J. D. Chestnut, *Biotechnol. Lett.*, 2016, **38**, 919–929.
69 H. T. Lv, S. B. Zhang, B. Wang, S. H. Cui and J. Yan, *J. Controlled Release*, 2006, **114**, 100–109.
70 M. Sadelain, E. P. Papapetrou and F. D. Bushman, *Nat. Rev. Cancer*, 2011, **12**, 51–58.
71 B. K. Lundholt, K. M. Scudder and L. Pagliaro, *J. Biomol. Screening*, 2003, **8**, 566–570.
72 C. J. Marshall, *Cell*, 1995, **80**, 179–185.
73 V. Gray-Schopfer, C. Wellbrock and R. Marais, *Nature*, 2007, **445**, 851–857.
74 A. A. Samatar and P. I. Poulikakos, *Nat. Rev. Drug Discovery*, 2014, **13**, 928–942.
75 C. Wellbrock, M. Karasarides and R. Marais, *Nat. Rev. Mol. Cell Biol.*, 2004, **5**, 875–885.
76 C. K. Weber, J. R. Slupsky, H. A. Kalmes and U. R. Rapp, *Cancer Res.*, 2001, **61**, 3595–3598.
77 V. Emuss, M. Garnett, C. Mason, R. Marais and C. G. Project, *Cancer Res.*, 2005, **65**, 9719–9726.
78 S. Wilhelm, C. Carter, M. Lynch, T. Lowinger, J. Dumas, R. A. Smith, B. Schwartz, R. Simantov and S. Kelley, *Nat. Rev. Drug Discovery*, 2006, **5**, 835–844.
79 J. H. Hu, S. M. Miller, M. H. Geurts, W. X. Tang, L. W. Chen, N. Sun, C. M. Zeina, X. Gao, H. A. Rees, Z. Lin and D. R. Liu, *Nature*, 2018, **556**, 57–63.
80 B. Zetsche, J. S. Gootenberg, O. O. Abudayyeh, I. M. Slaymaker, K. S. Makarova, P. Essletzbichler, S. E. Volz, J. Joung, J. van der Oost, A. Regev, E. V. Koonin and F. Zhang, *Cell*, 2015, **163**, 759–771.
81 M. Zheng, H. J. Xu, X. H. Liao, C. P. Chen, A. L. Zhang, W. X. Lu, L. Wang, D. Y. Yang, J. C. Wang, H. K. Liu, X. Z. Zhou and K. P. Lu, *Oncotarget*, 2017, **8**, 29771–29784.

